

# Quantum Interference and Decoherence in Single-Molecule Junctions: How Vibrations Induce Electrical Current

R. Härtle<sup>1</sup>, M. Butzin<sup>1</sup>, O. Rubio-Pons<sup>1,2</sup>, and M. Thoss<sup>1</sup>

<sup>1</sup> *Institut für Theoretische Physik und  
Interdisziplinäres Zentrum für Molekulare Materialien,  
Friedrich-Alexander-Universität Erlangen-Nürnberg,  
Staudtstr. 7/B2, D-91058 Erlangen, Germany*

<sup>2</sup> *Theoretische Chemie, Technische Universität München,  
Lichtenbergstr. 4, D-85747 Garching, Germany*

(Dated: January 12, 2013)

## Abstract

Quantum interference effects and decoherence mechanisms in single-molecule junctions are analyzed employing a nonequilibrium Green's function approach. Electrons tunneling through quasi-degenerate states of a nanoscale molecular junction exhibit interference effects. We show that electronic-vibrational coupling, inherent to any molecular junction, strongly quenches such interference effects. As a result, the electrical current can be significantly larger than without electronic-vibrational coupling. The analysis reveals that the quenching of quantum interference is particularly pronounced if the junction is vibrationally highly excited, e.g. due to current-induced nonequilibrium effects in the resonant transport regime.

PACS numbers: 73.23.-b, 85.65.+h, 71.38.-k

Quantum interference is at the heart of quantum mechanics. While this classically counter-intuitive phenomenon has been verified long ago, *e.g.* by double-slit experiments [1, 2], quantum interference effects recently attracted much attention in electron transport through nanostructures, such as, *e.g.*, quantum dots [3–7] or single-molecule junctions [8–11]. When a molecule is contacted by two electrodes, forming a single-molecule junction [12, 13], two different physical regimes become interconnected: The microscopic realm of a single molecule, governed by coherent quantum dynamics, and macroscopic reservoirs of electrons, wherein electronic coherences decay rapidly. Hence, the question arises to which extent a single-molecule junction preserves quantum coherence and which decoherence mechanisms are active. Understanding these mechanisms is crucial for the design of nanoelectronic devices.

This question can be addressed by analyzing quantum interference effects that occur in a single-molecule junction. Consider *e.g.* the model molecular junction depicted in Fig. 1a. This junction comprises two electronic states, which are located at the molecular bridge. One of them is *gerade* with respect to the  $L \leftrightarrow R$  symmetry of the junction, the other is *ungerade*. If these states are quasi-degenerate, they provide, similar to a double-slit experiment, two different pathways for an electron tunneling through the junction. As the respective wave-functions for the outgoing electron thus differ by sign, they destructively interfere with each other. As a result, the corresponding tunnel current is suppressed, or may even completely vanish (*vide infra*). In this letter we show that such quantum interference effects are quenched by vibrationally-assisted tunneling processes (cf. Fig. 1b and 1c), during which the tunneling electron excites or deexcites vibrational degrees of freedom of the junction. Due to the small size and mass of a molecular conductor, vibrational and electronic degrees of freedom are typically strongly coupled, resulting in inelastic tunneling processes, which strongly influence the respective transport characteristics [13–20]. This aspect distinguishes nanoscale molecular conductors from mesoscopic systems and quantum dots.

We describe vibrationally coupled electron transport through a single molecule (M) that is covalently bound to two metal leads (L,R) by a generic model with Hamiltonian  $H =$

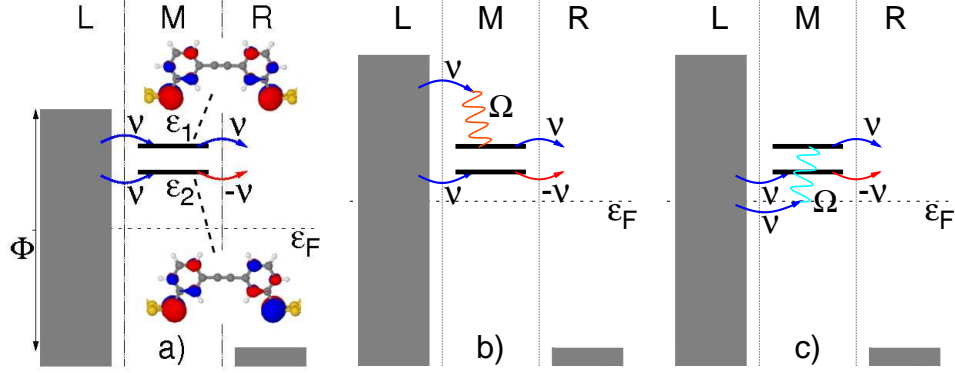


FIG. 1: (Color online) a): Scheme of a molecular junction at a finite bias voltage  $\Phi$  that exhibits destructive interference. The gray shaded areas depict the continuum of occupied electronic states in the left (L) and the right (R) lead. Electronic states located at the molecular bridge (M) are represented by black bars. The blue and red arrows depict the coupling of these states to the leads, which due to the different symmetry of the corresponding orbitals, *gerade* and *ungerade*, differ by sign (example orbitals are given in the insets). b) and c): Example processes for vibrational excitation (red wiggly line) and deexcitation (blue wiggly line) upon inelastic tunneling of an electron through the molecular junction.

$H_{\text{el}} + H_{\text{vib}}$ , where ( $\hbar = 1$ )

$$H_{\text{el}} = \sum_{i \in \text{M}} \epsilon_i c_i^\dagger c_i + \sum_{k \in \text{L,R}} \epsilon_k c_k^\dagger c_k + \sum_{k,i} (V_{ki} c_k^\dagger c_i + \text{H.c.}), \quad (1)$$

$$H_{\text{vib}} = \sum_{\alpha} \Omega_{\alpha} a_{\alpha}^{\dagger} a_{\alpha} + \sum_{\alpha,i} \lambda_{i\alpha} (a_{\alpha} + a_{\alpha}^{\dagger}) c_i^{\dagger} c_i. \quad (2)$$

The electronic part of the Hamiltonian,  $H_{\text{el}}$ , includes electronic states with energies  $\epsilon_i$  located at the molecular bridge (cf. Fig. 1a). These states are coupled by interaction matrix elements  $V_{ki}$  to electronic states with energies  $\epsilon_k$  in the leads. Thereby, the operators  $c_i^{\dagger}/c_i$  ( $c_k^{\dagger}/c_k$ ) represent the respective creation/annihilation operators for the states of the molecular bridge (the leads). The vibrational degrees of freedom of the junction are described as harmonic oscillators with frequencies  $\Omega_{\alpha}$ , and corresponding creation/annihilation operators  $a_{\alpha}^{\dagger}/a_{\alpha}$ . Here,  $\lambda_{i\alpha}$  denotes the electronic-vibrational (vibronic) coupling strength between vibrational mode  $\alpha$  and the  $i$ th state of the bridge.

To study quantum interference and decoherence effects in molecular junctions, we employ a Non-Equilibrium Green's Function approach (NEGF) [14–17, 21]. NEGF theory allows to describe quasi-degenerate molecular levels, which is crucial for the analysis of the

respective quantum interference effects. The method is based on (self-consistent) second-order perturbation theory in the molecule-lead coupling, and treats electronic-vibrational coupling non-perturbatively. The details of our NEGF approach have been outlined previously [14–16, 21]. Briefly, the approach is based on the small polaron transformation [15, 17, 21]. The accordingly transformed Hamiltonian  $\overline{H}$  comprises a polaron-shift of the electronic states of the molecular bridge,  $\overline{\epsilon}_i = \epsilon_i - \sum_{\alpha} (\lambda_{i\alpha}^2 / \Omega_{\alpha})$ , a molecule-lead coupling term, which is renormalized by the shift operators  $X_i = \exp(\sum_{\alpha} (\lambda_{i\alpha} / \Omega_{\alpha}) (a_{\alpha} - a_{\alpha}^{\dagger}))$ , and Hubbard-like electron-electron interaction terms,  $(\lambda_{i\alpha} \lambda_{j\alpha} / \Omega_{\alpha}) c_i^{\dagger} c_i c_j^{\dagger} c_j$ , but no direct electronic-vibrational coupling terms. The vibrationally induced electron-electron interactions are treated using a non-perturbative approximate scheme [14]. In the (anti-)adiabatic regime of a molecular junction, the electronic Green's function matrix  $\mathbf{G}$  can be described as  $\mathbf{G}_{ij}(\tau, \tau') \approx \mathbf{G}_{c,ij}(\tau, \tau') \langle T_c X_i(\tau) X_j^{\dagger}(\tau') \rangle$ . The matrix  $\mathbf{G}_{c,ij}(\tau, \tau') = -i \langle T_c c_i(\tau) c_j^{\dagger}(\tau') \rangle$  is determined by the self-energy matrix  $\Sigma_{L/R,ij}(\tau, \tau') = \sum_{k \in L/R} V_{ki}^* V_{kj} g_k(\tau, \tau') \langle T_c X_j(\tau') X_i^{\dagger}(\tau) \rangle$ , where  $g_k$  denotes the free Green's function of lead state  $k$  and  $T_c$  is the time-ordering operator on the Keldysh contour. The correlation functions of the shift-operators  $X_i$  are evaluated using a cumulant expansion in the dimensionless coupling parameters  $\lambda_{i\alpha} / \Omega_{\alpha}$ , which in turn requires the electronic Green's functions  $\mathbf{G}_{c,ij}$ . Therefore, we employ a self-consistent solution scheme [15, 21]. This scheme accounts for the molecule-lead coupling in second-order (self-consistent) perturbation theory. It is thus exact for vanishing vibronic coupling, and due to the small polaron transformation, also for vanishing molecule-lead coupling. The electrical current through the junction is given by  $I = 2e \int (d\epsilon / (2\pi)) \text{tr} \{ \Sigma_L^< \mathbf{G}_c^> - \Sigma_L^> \mathbf{G}_c^< \}$  [14, 15, 21].

First, we consider a generic model system similar to the one depicted in Fig. 1a with parameters that are typical for single-molecule junctions. The model comprises two electronic states located at  $\overline{\epsilon}_1 = 0.404 \text{ eV}$  and  $\overline{\epsilon}_2 = 0.4 \text{ eV}$  above the Fermi-level  $\epsilon_F = 0$ . State 1 of our model system is coupled to the vibrational mode with coupling strength  $\lambda_1 = 0.06 \text{ eV}$ . For state 2, we consider  $\lambda_2 = 0$ . This choice simplifies the analysis of the corresponding decoherence mechanism, which occurs in general for  $\lambda_1 \neq \lambda_2$ . These states are coupled to the leads in the same way as shown in Fig. 1a, *i.e.* with  $\nu_{L,1/2} = \nu_{R,1} = -\nu_{R,1} = \nu = 0.1 \text{ eV}$ . The leads are modelled as semi-infinite tight-binding chains with level-width functions  $\Gamma_{L/R,ij}(\epsilon) = (\nu_{L/R,i} \nu_{L/R,j} / \gamma^2) \text{Re} [\sqrt{4\gamma^2 - (\epsilon - \mu_{L/R})^2}]$  and  $\gamma = 3 \text{ eV}$ . The bias voltage  $\Phi$  is assumed to symmetrically drop at the contacts,  $\mu_L = -\mu_R = \Phi/2$ .

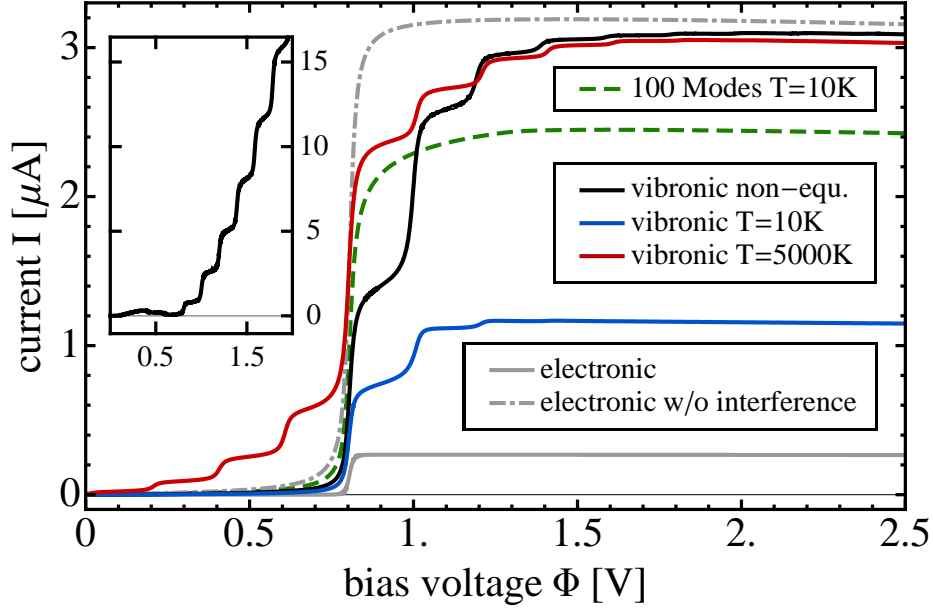


FIG. 2: (Color online) Current-voltage characteristics for a generic model molecular junction that exhibits two destructively interfering electronic states (see Fig. 1) coupled to a single vibrational mode. The inset shows the corresponding vibrational excitation characteristics,  $\langle a^\dagger a \rangle$ .

Current-voltage characteristics for this model system are shown in Fig. 2. Thereby, the solid gray line shows the electrical current obtained for static nuclei ('electronic current'), *i.e.* for the polaron-shifted electronic states with  $\lambda_1 = 0$ . The comparatively small value of the electronic current ( $0.26 \mu\text{A}$  for  $\Phi > 2\bar{\epsilon}_{1/2}$ ) is a result of destructive interference effects in this molecular junction, which arise due to the symmetry of the molecule-lead coupling and the quasidegeneracy of the two states ( $\bar{\epsilon}_1 - \bar{\epsilon}_2 \lesssim \Gamma$ ). If the partial currents corresponding to the different pathways through the molecular junction are added incoherently (dashed gray line), a much larger value ( $3.2 \mu\text{A}$  for  $\Phi > 2\bar{\epsilon}_{1/2}$ ) is obtained. This demonstrates the presence of destructive quantum interference, which reduces the current through this junction by more than an order of magnitude.

If we take into account electronic-vibrational coupling,  $\lambda_1 = 0.06 \text{ eV}$ , vibrational excitation and deexcitation processes (cf. Fig. 1b and 1c) contribute to the electron transport through the junction [14, 15, 15–17]. These inelastic processes result in an highly excited state of the vibrational mode for  $\Phi \gtrsim 2\epsilon_1$  (cf. the vibrational excitation characteristics shown in the inset of Fig. 2). The respective current-voltage characteristics, which is depicted by

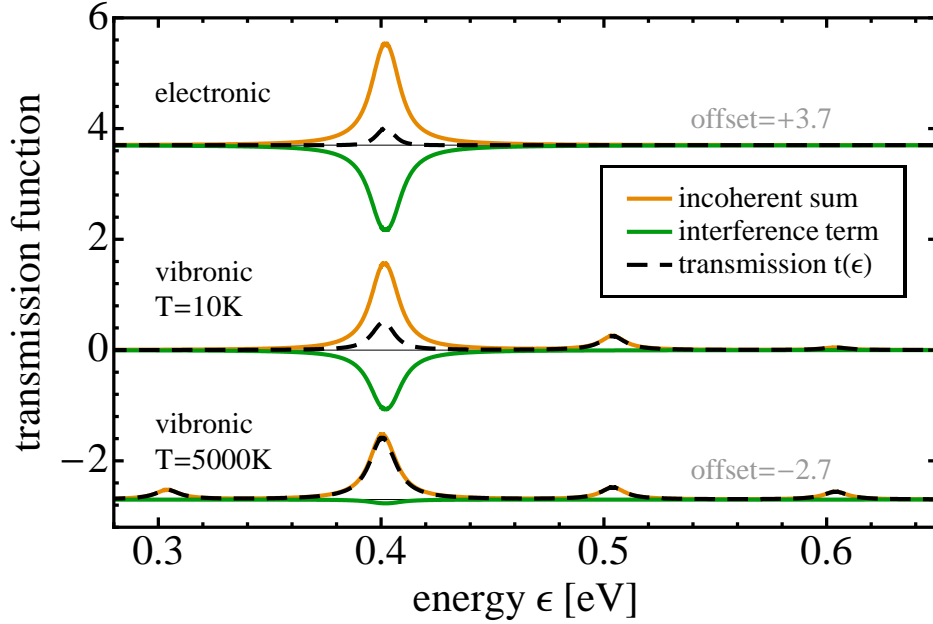


FIG. 3: (Color online) Transmission functions  $t(\epsilon)$  (dashed black line) corresponding to the currents depicted by the solid gray, blue and red lines in Fig. 2 at a high bias voltage. For clarity, the graphs for these three different cases are separated by offsets. In addition, the incoherent sum of transmission channels  $t_{\text{sum}}(\epsilon)$  (orange lines) and the interference term  $t_{\text{int}}(\epsilon)$  (green lines) are depicted (cf. Eqs. (3)).

the solid black line in Fig. 2, exhibits several steps at  $\Phi = 2(\bar{\epsilon}_1 + n\Omega)$ ,  $n \in \mathbb{N}$ , corresponding to vibrationally-assisted electron transport processes [14–17]. Intriguingly, the current that is obtained including electronic-vibrational coupling (black line), is much larger than the electronic current (gray line) and approaches the value obtained by incoherent summation of the different electronic pathways (dashed gray line). Electronic-vibrational coupling thus results in a complete quenching of destructive interference effects in this model molecular junction, or equivalently, leads to strong decoherence. While the results discussed so far have been obtained using the full current-induced nonequilibrium vibrational distribution, the basic mechanism of vibronic decoherence can also be described within the often employed approximation, where the state of the vibrational mode is restricted to its thermal equilibrium state after each electron transmission event. The solid blue and red lines in Fig. 2 show results employing this simpler approach obtained for temperatures of 10 K and 5000 K [22], respectively.

To analyze these effects in more detail we employ a thermal equilibrium state for the vibration and consider bias voltages  $\Phi \gg \epsilon_{1/2}$ , for which the current can be expressed in a form similar to Landauer theory,  $I \approx 2e \int_{-\infty}^{\infty} (d\epsilon/2\pi) t(\epsilon)$ , with the transmission function  $t(\epsilon) \equiv i \text{tr}\{\mathbf{\Gamma}_L \mathbf{G}^>\}$ . This transmission function  $t(\epsilon)$  can be split into an incoherent sum of transmission channels,  $t_{\text{sum}}(\epsilon) = i \sum_i \tilde{\mathbf{G}}_{ii}^> \mathbf{\Gamma}_{L,ii}$ , where  $\tilde{\mathbf{G}}_{ii}^>$  is evaluated disregarding the off-diagonal elements of  $\mathbf{\Sigma}_{L/R}$ , and an interference term,  $t_{\text{int}}(\epsilon) = t(\epsilon) - t_{\text{sum}}(\epsilon)$ . The interference term explicitly shows the interference effects between individual transmission channels encoded in the off-diagonal elements of  $\mathbf{\Sigma}_{L/R}$ . For our specific model system, in the wide-band approximation with  $\Gamma = 2\nu^2/\gamma$ , we obtain

$$\begin{aligned} t_{\text{sum}}(\epsilon) &= (\Gamma/|\epsilon - \bar{\epsilon}_2 + i\Gamma|)^2 \\ &+ A \sum_{l=-\infty}^{\infty} I_l(x) e^{\beta l \Omega/2} (\Gamma/|\epsilon - \bar{\epsilon}_1 - l\Omega + i\Gamma|)^2, \\ t_{\text{int}}(\epsilon) &= -2A\Gamma^2 \text{Re} [(\epsilon - \bar{\epsilon}_1 + i\Gamma)^{-1} (\epsilon - \bar{\epsilon}_2 - i\Gamma)^{-1}]. \end{aligned} \quad (3)$$

Thereby, the prefactor  $A = e^{-(\lambda_1^2/\Omega^2)(2N_{\text{vib}}+1)}$  is determined by the average vibrational excitation  $N_{\text{vib}} = (e^{\beta\Omega} - 1)^{-1}$  and the inverse temperature  $\beta = (k_B T)^{-1}$ , while  $I_l(x) = I_l(2(\lambda_1^2/\Omega^2)\sqrt{N_{\text{vib}}(N_{\text{vib}}+1)})$  denotes the  $l$ th modified Bessel function of the first kind.

Fig. 3 shows the transmission functions (dashed black lines) corresponding to the currents represented by the gray, the solid blue and red line in Fig. 2. In addition to the transmission functions, the incoherent sum of transmission channels (orange line) and the interference terms (green line) are depicted. Two important observations can be made. First, for non-vanishing vibronic coupling, the transmission peak associated with state 1 is fragmented into vibrational side-peaks. These side-peaks, which are associated with vibronic tunneling processes (Fig. 1b and 1c), appear in the incoherent sum of transmission channels, but not in the interference term. Thus, these side-peaks can directly contribute to the total transmission probability. Second, the prefactor  $A = e^{-(\lambda_1^2/\Omega^2)(2N_{\text{vib}}+1)}$  reduces the main peak at  $\epsilon \approx \bar{\epsilon}_{1/2}$  in both parts of the transmission function. While for  $N_{\text{vib}} \rightarrow \infty$  the elastic peak in the incoherent sum of the transmission channels is thus halved, the peak in the interference term completely vanishes for a high level of vibrational excitation. As a result, quantum interference effects are greatly reduced, if the vibration acquires a highly excited state, in particular in the resonant tunneling regime (cf. the inset of Fig. 2).

In the model considered so far, the decoherence mechanism is based on the coupling of the electronic states of the molecular junction to its internal vibrational degrees of freedom.

In many cases [23, 24], however, decoherence (or dephasing) is a result of external or environmental degrees of freedom. Such a mechanism can be described by a different model, where the electronic states are coupled to a bath of harmonic oscillators, mimicking, e.g., the coupling to the phonons in the leads [25] or a surrounding solvent in an electrochemically gated molecular junction [25, 26]. The current-voltage characteristics obtained for such a model is shown in Fig. 2 by the dashed green line. Thereby, the overall vibronic coupling strength (as specified by the reorganization energy, 0.36 meV) is the same as for the single-mode model considered above but has been equally distributed over 100 vibrational modes, which frequencies range from 1 meV to 250 meV with an equidistant spacing of 2.5 meV. The comparison to the corresponding single-mode case (solid blue line) shows that the coupling to a multitude of vibrational modes induces even stronger decoherence effects. Within the analysis of interference discussed above, this mechanism is encoded in the prefactor  $A$  of Eqs. (3), which for the present model reads  $A = e^{-\sum_{\alpha}(\lambda_{1\alpha}^2/\Omega_{\alpha}^2)(2N_{\text{vib},\alpha}+1)}$ . Due to the low-frequency modes, it is considerably smaller than for the single-mode model.

The results discussed so far for a generic model system show that electronic-vibrational coupling leads to decoherence in single-molecule junctions and elucidates the underlying mechanisms. As a specific example for a single-molecule junction that exhibits quantum interference and decoherence, we consider a *o*-biphenylacetylenedithiolate molecule bound to gold electrodes (see Fig. 4). The model parameters of this junction were determined by first-principles electronic structure calculations, where a detailed description of our methodology can be found in Ref. [27]. The junction exhibits 36 active vibrational modes coupled to a multitude of closely-lying electronic states that interfere with each other. Test calculations show that for bias voltages within a range of  $|\Phi| \lesssim 3 \text{ V}$  the three electronic states corresponding to the molecular orbitals depicted in Fig. 4a) are sufficient to describe the electronic current in this junction. The comparison of the electronic current obtained within this three-state model (solid gray line) with the significantly larger current that is obtained for the transport through the individual states (dashed lines) demonstrates the presence of pronounced interference effects among the three pathways in this junction. Analysis shows that the destructive interference of the highest occupied molecular orbital (HOMO) and HOMO-1 are due to their quasidegeneracy and the fact that their wavefunctions are symmetric and antisymmetric combinations, respectively. In addition, the electronic state corresponding to HOMO-4 exhibits destructive interference with the other two orbitals, due



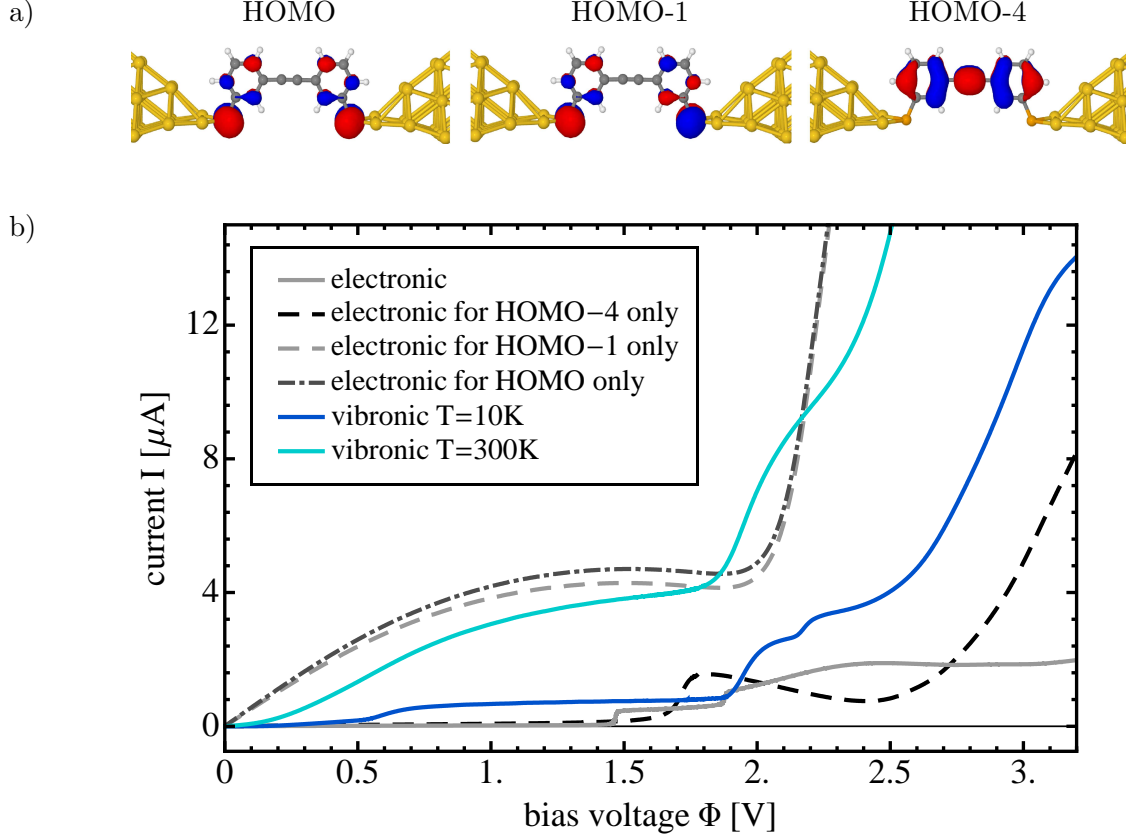


FIG. 4: (Color online) Electron Transport in an *o*-biphenylacetylenedithiolate molecular junction. a): relevant molecular orbitals, where the blue and the red color represent different signs. b): current-voltage characteristics for different scenarios as described in the legend.

to the broadening of the molecular levels. If we account for electronic-vibrational coupling, the current-voltage characteristics represented by the solid blue and turquoise line in Fig. 4 are obtained, where all 36 vibrational degrees of freedom are evaluated in thermal equilibrium at 10 K and 300 K, respectively. The associated current-voltage characteristics are significantly larger than the electronic current. Moreover, for an increasing temperature of the vibrational modes, the current through the junction approaches the significantly higher values obtained for the individual channels, given by the dashed lines. As in the generic model system, vibronic interactions thus result in a strong decoherence of interfering electronic states, which is greatly enhanced by the temperature of the modes or equivalently their level of vibrational excitation.

In summary, single-molecule junctions often exhibit multiple closely-lying electronic states

that provide interfering pathways for the tunneling of electrons. Our analysis, obtained for both a generic model and a specific example, show that electronic-vibrational coupling leads to decoherence and quenching of these electronic quantum interference effects. As a result, the electrical current in molecular junctions can be significantly larger than without electronic-vibrational coupling. This effect is particularly pronounced if the junction is vibrationally highly excited, e.g. due to current-induced nonequilibrium effects in the resonant transport regime. It should also be emphasized that this decoherence mechanism is an intrinsic property of a single-molecule junction.

We gratefully acknowledge fruitful discussions with S. Ballmann, B. Kubala and P. B. Coto, and generous allocation of computing time by the Leibniz Rechenzentrum München (LRZ). The work at the Friedrich-Alexander Universität Erlangen-Nürnberg was carried out in the framework of the Cluster of Excellence "Engineering of Advanced Materials".

- 
- [1] Möllenstedt and Düker, Z. Physik **145**, 377 (1956).
  - [2] O. Nairz, M. Arndt, and A. Zeilinger, Am. J. Phys. **71**, 319 (2002).
  - [3] A. W. Holleitner, C. R. Decker, H. Qin, K. Eberl, and R. H. Blick, Phys. Rev. Lett. **87**, 256802 (2001).
  - [4] B. Kubala and J. König, Phys. Rev. B **65**, 245301 (2002).
  - [5] A. Donarini, G. Begemann, and M. Grifoni, Phys. Rev. B **82**, 125451 (2010).
  - [6] A. Ueda, O. Entin-Wohlman, M. Eto, and A. Aharony, Phys. Rev. B **82**, 245317 (2010).
  - [7] T. Markussen, R. Stadler, and K. S. Thygesen, Nano Lett. **10**, 4260 (2010).
  - [8] G. C. Solomon, A. Gagliardi, A. Pecchia, T. Frauenheim, A. Di Carlo, J. R. Reimers, and N. S. Hush, Nano Lett. **6**, 2431 (2006).
  - [9] M. G. Schultz, Phys. Rev. B **82**, 155408 (2010).
  - [10] D. Darau, G. Begemann, A. Donarini, and M. Grifoni, Phys. Rev. B **79**, 235404 (2009).
  - [11] D. Brisker, I. Cherkes, C. Gnodtke, D. Jarukanont, S. Klaiman, W. Koch, S. Weissmann, R. Volkovich, M. Caspary Toroker, and U. Peskin, Mol. Phys. **106**, 281 (2008).
  - [12] J. C. Cuevas and E. Scheer, *Molecular Electronics: An Introduction To Theory And Experiment* (World Scientific, Singapore, 2010).
  - [13] M. Galperin, M. A. Ratner, and A. Nitzan, J. Phys.: Condens. Matter **19**, 103201 (2007).

- [14] R. Härtle, C. Benesch, and M. Thoss, Phys. Rev. Lett. **102**, 146801 (2009).
- [15] R. Härtle, C. Benesch, and M. Thoss, Phys. Rev. B **77**, 205314 (2008).
- [16] R. Härtle, R. Volkovich, M. Thoss, and U. Peskin, J. Chem. Phys. **133**, 081102 (2010).
- [17] R. Härtle and M. Thoss, arXiv:1010.4993 (2010).
- [18] K. Flensberg, Phys. Rev. B **68**, 205323 (2003).
- [19] A. Mitra, I. Aleiner, and A. J. Millis, Phys. Rev. B **69**, 245302 (2004).
- [20] M. C. Lüffe, J. Koch, and F. von Oppen, Phys. Rev. B **77**, 125306 (2008).
- [21] M. Galperin, A. Nitzan, and M. A. Ratner, Phys. Rev. B **73**, 045314 (2006).
- [22] At 5000 K the average thermal excitation of the vibrational mode is comparable to the one obtained by the full nonequilibrium calculation (cf. the inset of Fig. 2).
- [23] J. Lehmann, S. Kohler, V. May, and P. Hänggi, J. Chem. Phys. **121**, 2278 (2004).
- [24] D. Segal, A. Nitzan, W. B. Davis, M. R. Wasielewski, and M. A. Ratner, J. Phys. Chem. B **104**, 3817 (2000).
- [25] R. Jorn and T. Seidemann, J. Chem. Phys. **131**, 244114 (2009).
- [26] N. J. Tao, Nat. Nano. **1**, 173 (2006).
- [27] C. Benesch, M. Cizek, J. Klimes, M. Thoss, and W. Domcke, J. Phys. Chem. C **112**, 9880 (2008).